Non-Local finite element to model the compressive behavior of composite structures

A. BETTADAHALLI[a], J-C. GRANDIDIER[b]

a. Institut Pprime, UPR CNRS 3346, ISAE-ENSMA, University of Poitiers, ISAE-ENSMA - Téléport2 - 1 Av. Clément Ader - BP40109, F-86962 Futuroscope Chasseneuil Cedex, e-mail : anil.bettadahalli-channakeshava@ensma.fr

b. Institut Pprime, UPR CNRS 3346, ISAE-ENSMA, University of Poitiers, ISAE-ENSMA - Téléport2 - 1 Av. Clément Ader - BP40109, F-86962 Futuroscope Chasseneuil Cedex, e-mail : grandidier@ensma.fr

…

Résumé :

Cet article propose un modèle numérique homogénéisé d'éléments finis non locaux, similaire à la théorie du gradient II de Mindlin [1], pour évaluer la résistance à la compression des composites fibres longues carbone / époxy à l'échelle mésoscopique / structurelle. Le cadre de cette modélisation non locale est plus général que celui de [2] pour simuler le phénomène de microbuckling dans les composites UD et tissés. Le modèle numérique non local développé est implémenté dans le sous-programme User Elément (UEL) d'ABAQUS ©, ce qui permet de simuler le comportement de cas 2D et 3D. Un 2D élément non locale (NL U32) super-paramétrique continu (C^1) *est développé pour le cas élastique isotrope linéaire. Différents résultats de tests sont présentés pour valider le modèle FE non local pour les cas 2D, en comparant les résultats d'un élément non local homogénéisé avec un élément iso-paramétrique d'Abaqus et en comparant le comportement mécanique avec une microstructure composite 2D discrétisée à l'aide d'éléments classiques d'ABAQUS ©.*

Abstract :

A homogenized non-local finite element model is proposed in this article, similar to Mindlin's II gradient theory [1] to assess the compressive strength of the carbon/epoxy long fiber composite at the mesoscopic/structural scale. The framework of this non-local modelling is more general that of [2] to assess microbuckling phenomenon in UD and woven composites. The developed nonlocal numerical model is implemented in User Element (UEL) subroutine for analysis in ABAQUS ©, which permits to simulate the behavior of 2D and 3D cases. A 2D continuous (C^1) *super-parametric non-local element (NL U32) is developed for linear isotropic elastic case. Various tests results are presented to validate the non-local FE model for 2D cases, by comparing results of homogenized non-local element with ABAQUS © iso-paramteric element and then by comparing mechanical behavior/response with 2D composite microstructure, modelled using ABAQUS © classical elements.*

Mots clefs : Nonlocal model, Compression, Long-fiber composites

1 Introduction

Composite materials continue to gain popularity in various industries like aerospace, automotive, naval, medical, etc. primarily due to their ability to reduce weight. One of the main advantages of composite materials is that they can be designed to obtain a wide range of properties by altering the type and ratios of constituent materials, their orientations, process parameters, and so on. Composites also have high mechanical properties with a low weight, which makes them ideal materials for automotive and aerospace applications. Other advantages of composites include high fatigue resistance, toughness, thermal conductivity and corrosion resistance. The main disadvantage of composites is the high processing costs, which limit their wide-scale usage.

The compressive failure of long carbon fiber composites is due to complex mechanisms. The knowledge of this material is important for the design of composite structures [3], because the compressive strength and stiffness of laminates is assumed less than their tensile strength. The damage mechanism in long fiber composites is complex and depends on many parameters. Competing modes of compressive failure exist, including *delamination, fiber failure and elastic and plastic microbuckling*. '*Elastic microbuckling'* is a shear buckling instability and the matrix deforms in simple shear, whereas '*Plastic microbuckling'* is also a shear buckling instability, which occurs at sufficiently large strains for the matrix to deform in non-linear manner [4].

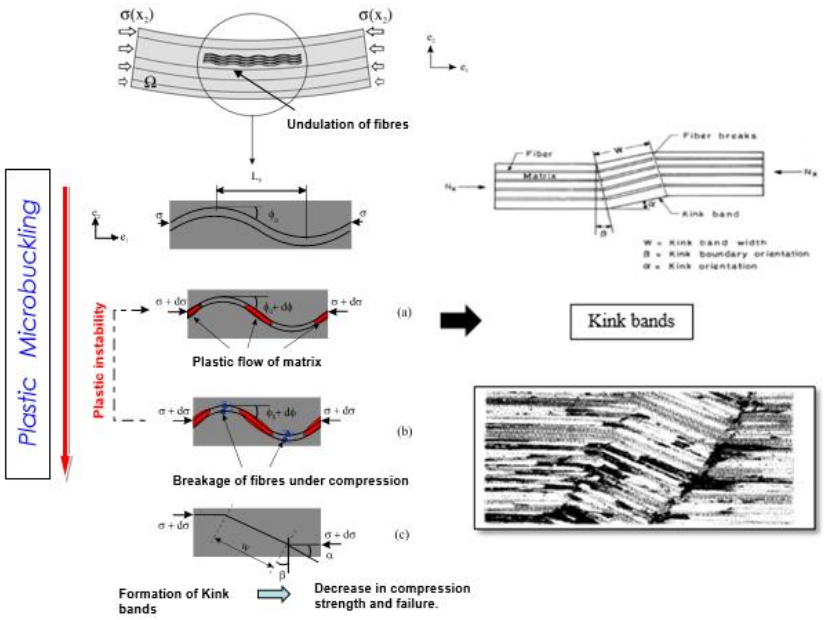

Figure 1: Plastic microbuckling phenomenon in UD composites[2]

Many experimental investigations conducted by various researchers over the years (*UD composites*: [5-7]; *Woven composites*: [8-10]) confirmed that, *composite with fibers having initial misalignments*, when loaded under compression, the shear stresses are influenced by the angle between fibers and loading directions. Resin (epoxy matrix) maintains the fiber misalignment. But, when the compressive load increases, the fiber transmits to the matrix a non-linear shear load. As the matrix has non-linear behavior, the loss of stiffness increases the initial fiber misalignment, the microbuckling appears. When fiber deformation reaches higher than critical value, formation of kink band/shear band occurs (see Fig. 1). Consequently, this leads to decrease in compression strength and failure of composite. Therefore, the

main parameters that influence the microbuckling and kink band formation are: a) Matrix physical non-linearity and b) Presence of fiber initial wavy imperfection/undulation. There are many articles in the literature regarding the modeling of composites compressive behavior, particularly the microbuckling phenomenon as a local instability of UD composites (local models: [11- 14]). However, each model is limited to particular cases and only few researchers modeled the mechanism at the structural / mesoscopic scale (Non-local models: [15-19]). For example, Drapier et al. [2], proposed a 2D homogenized model (1), which takes into account fiber initial alignment defects, matrix plasticity and structural parameters.

$$-\int_{\Omega}\{f E_f\, r_{gf}^2 v''\, \delta v'' + \boldsymbol{S}\cdot\delta\boldsymbol{E}\}d\Omega + \langle \boldsymbol{F}\cdot\delta\boldsymbol{u}\rangle = 0 \qquad \forall\delta\boldsymbol{u} \tag{1}$$

Where, f is fiber volume fraction, E_f is fiber Yong's modulus, $r_{gf}=\sqrt{\frac{I}{S_f}}$ is fiber gyration radius, v'' is fiber curvature field, $\boldsymbol{S}$ is Second Piola Kirchhoff stress tensor, $\boldsymbol{E}$ is the Green Lagrange strain tensor. The model is successful in predicting the elastic microbuckling modes, but the model is 2D and assumes that, the microbuckling is periodic in fiber direction, just one gradient in thickness direction is taken into account. Consequently, not possible to compare test results obtained with real 3D structures. Moreover, the prediction of both the 'distribution' and 'amplitudes' of fiber initial imperfection is still not well known [20]. Hence, it is necessary to extend the model of Drapier et al. [2]. Also there is no particular model that has been developed to assess the compressive strength on complex structure with UD and woven composites (2D and 3D), which takes into account the effects of gradients.

Therefore, a new homogenized non-local finite element model is proposed, more general of [2] to simulate compressive behavior of composite materials at macro/mesoscopic scale, which permits to take into account the microstructural effects. The developed non-local numerical model is implemented in User Element (UEL) subroutine for analysis in ABAQUS ©, which permits to simulate the behavior of 2D and 3D cases. At present, a 2D continuous (C^1) super-parametric non-local element (NL U32) is developed for linear isotropic elastic case (both the matrix and fiber is assumed to be isotropic and elastic). Nonlinearities (geometrical and material) will be implemented in the element in near future and then extension to the development of 3D non-local element.

The theoretical and numerical parts of the model are presented in the section 2. Validation of the developed finite element for 2D case is performed by comparing results of homogenized non-local super-parametric element with one ABAQUS © iso-paramteric elements and then by comparing mechanical behavior/response with 2D composite microstructure, modelled using ABAQUS © elements as a final validation (section 3).

2 Homogenized Non-Local numerical model

2.1 Theoretical part

From (1), it is understood that, it takes into account only the transverse fiber curvature field ($v'' = \frac{\partial^2 v}{\partial x^2}$) along just one direction (UD) as shown in Fig. 2.

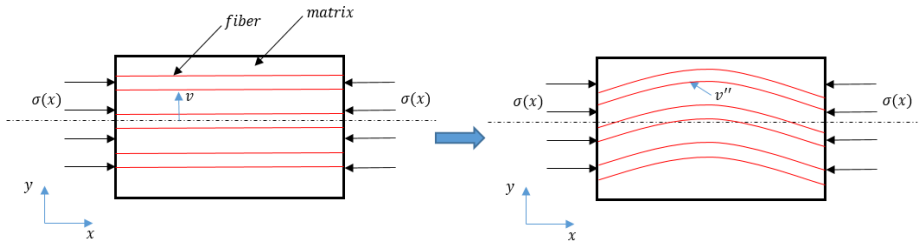

Figure 2: UD Ply loaded under compression

The energy of local bending corresponds to the first term in (1). This term has been obtained by Gardin et al. [6] with an asymptotic development. But, it is very restrictive, and corresponds to just UD ply under compression. Therefore, it is necessary to extend the model for more general realistic case, taking into account the fiber curvature field in more complex mesostructure, for example: 2D and 3D woven, where fiber curvature field is not only restricted in one direction, but are randomly oriented in multiple directions, during compression or torsion-compression, as shown in (Fig . 3):

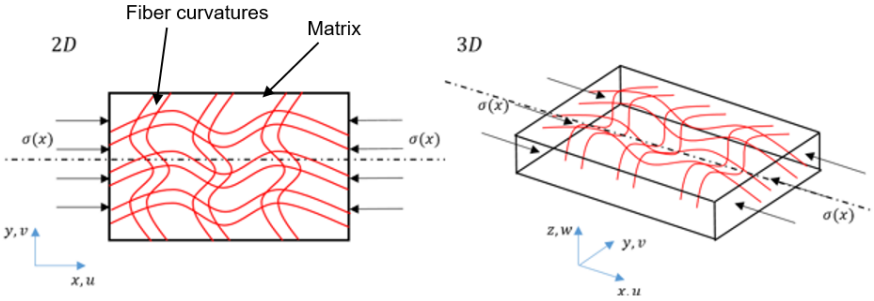

Figure 3: 2D and 3D woven composite with fibers curvatures in multiple directions loaded under compression

In the Mindlin's second order strain gradient theory [1], both curvature and strain generate an energy of deformation. Hence, this theory is used as a main reference to develop our homogenized nonlocal model. The kinematics is defined by the displacement field (classical), $\boldsymbol{u} = u(x,y,z)\boldsymbol{e}_1 + v(x,y,z)\boldsymbol{e}_2 + w(x,y,z)\boldsymbol{e}_3$ and the generalized fiber curvature field is defined by, $\boldsymbol{\kappa}$:

a) 2D

$$\boldsymbol{\kappa} = \left[\frac{\partial^2 u}{\partial x^2}, \frac{\partial^2 u}{\partial y^2}, \frac{\partial^2 u}{\partial x \partial y}, \frac{\partial^2 v}{\partial x^2}, \frac{\partial^2 v}{\partial y^2}, \frac{\partial^2 v}{\partial x \partial y}\right]_{2D}$$

b) 3D

$$\boldsymbol{\kappa} = \left[\frac{\partial^2 u}{\partial x^2}, \frac{\partial^2 u}{\partial y^2}, \frac{\partial^2 u}{\partial z^2}, \frac{\partial^2 u}{\partial x \partial y}, \frac{\partial^2 u}{\partial x \partial z}, \frac{\partial^2 u}{\partial y \partial z}, \frac{\partial^2 v}{\partial x^2}, \frac{\partial^2 v}{\partial y^2}, \frac{\partial^2 v}{\partial z^2}, \frac{\partial^2 v}{\partial x \partial y}, \frac{\partial^2 v}{\partial x \partial z}, \frac{\partial^2 v}{\partial y \partial z}, \frac{\partial^2 w}{\partial x^2}, \frac{\partial^2 w}{\partial y^2}, \frac{\partial^2 w}{\partial z^2}, \frac{\partial^2 w}{\partial x \partial y}, \frac{\partial^2 w}{\partial x \partial z}, \frac{\partial^2 w}{\partial y \partial z}\right]_{3D}$$

The new variables, $\boldsymbol{\kappa} = \kappa_{ijk}$, *the fiber curvature field or higher order bending strains* in multiple directions and $\overline{\overline{\boldsymbol{C_f}}}$, *the local fiber bending stiffness matrix* are introduced which depends on the complex mesostructure. Therefore, using principle of virtual work (PVW), a new variational formulation of homogenized non-local numerical model in order to assess microbuckling problem at mesoscopic scale is written as (2):

$$-\int_{\Omega\to 3D}\{\boldsymbol{\zeta}\cdot\delta\boldsymbol{\kappa}+\boldsymbol{S}:\delta\boldsymbol{E}\}d\Omega+\langle\boldsymbol{F}\cdot(\delta\boldsymbol{u}\,,\delta\boldsymbol{\kappa})\,\rangle=0\qquad\forall\delta\boldsymbol{u}\,,\forall\delta\boldsymbol{\kappa} \tag{2}$$

Where, $\boldsymbol{\zeta}$ is distributed bending moment (DBM) due to the fiber curvature fields, which leads to bending of fiber. It is related to the local fiber bending stiffness matrix by a linear law (3) as a first approximation, where, $\overline{\overline{\boldsymbol{C_f}}}$ contains a non-local parameters of the mesostructure material. Tensors: $\boldsymbol{S}$ is the Second Piola Kirchhoff stress tensor, $\boldsymbol{E}$ is the Green Lagrange strain tensor, and $\boldsymbol{F}$ is the generalized external load vector. The 1st term in (2) corresponds to '*internal fiber bending energy*', 2nd term corresponds to '*internal in-plane/classical strain energy*' and 3rd term corresponds to '*external efforts*'.

$$\boldsymbol{\zeta}=\overline{\overline{c_f}}\,\boldsymbol{\kappa} \tag{3}$$

The fiber bending energy term, $'\,\boldsymbol{\zeta}\cdot\delta\boldsymbol{\kappa}=\overline{\overline{c_f}}\,\boldsymbol{\kappa}\,\delta\boldsymbol{\kappa}\,'$ can be written in 3D as follows (4):

$$\begin{aligned}[\overline{\overline{c_f}}\,\boldsymbol{\kappa}\,\delta\boldsymbol{\kappa}\,]_{3D}=\;&A\frac{\partial^2u}{\partial x^2}\delta\left(\frac{\partial^2u}{\partial x^2}\right)+B\frac{\partial^2u}{\partial y^2}\delta\left(\frac{\partial^2u}{\partial y^2}\right)+C\frac{\partial^2u}{\partial z^2}\delta\left(\frac{\partial^2u}{\partial z^2}\right)+D\frac{\partial^2v}{\partial x^2}\delta\left(\frac{\partial^2v}{\partial x^2}\right)+E\frac{\partial^2v}{\partial y^2}\delta\left(\frac{\partial^2v}{\partial y^2}\right)+F\frac{\partial^2v}{\partial z^2}\delta\left(\frac{\partial^2v}{\partial z^2}\right)\\&+G\frac{\partial^2w}{\partial x^2}\delta\left(\frac{\partial^2w}{\partial x^2}\right)+H\frac{\partial^2w}{\partial y^2}\delta\left(\frac{\partial^2w}{\partial y^2}\right)+I\frac{\partial^2w}{\partial z^2}\delta\left(\frac{\partial^2w}{\partial z^2}\right)+J\frac{\partial^2u}{\partial x\partial y}\delta\left(\frac{\partial^2u}{\partial x\partial y}\right)+K\frac{\partial^2u}{\partial x\partial z}\delta\left(\frac{\partial^2u}{\partial x\partial z}\right)\\&+L\frac{\partial^2u}{\partial y\partial z}\delta\left(\frac{\partial^2u}{\partial y\partial z}\right)+M\frac{\partial^2v}{\partial x\partial y}\delta\left(\frac{\partial^2v}{\partial x\partial y}\right)+N\frac{\partial^2v}{\partial x\partial z}\delta\left(\frac{\partial^2v}{\partial x\partial z}\right)+O\frac{\partial^2v}{\partial y\partial z}\delta\left(\frac{\partial^2v}{\partial y\partial z}\right)\\&+P\frac{\partial^2w}{\partial x\partial y}\delta\left(\frac{\partial^2w}{\partial x\partial y}\right)+Q\frac{\partial^2w}{\partial x\partial z}\delta\left(\frac{\partial^2w}{\partial x\partial z}\right)+R\frac{\partial^2w}{\partial y\partial z}\delta\left(\frac{\partial^2w}{\partial y\partial z}\right)\end{aligned} \tag{4}$$

Where, $A,B,C,D,E,F,G,H,I,J,K,L,M,N,O,P,Q,R$ are the non-local mesostructure material parameters. Ganghoffer et al. [24] has proposed a methodology to identify these parameters with respect to Representative Volume Element (RVE) of woven materials.

2.1.1 Principle of virtual work and equilibrium equations (2D)

In this part, the development is proposed just for 2D case. For the convenience of the derivation, curvatures ($\boldsymbol{\kappa}=\kappa_{ijk}$) is written as:

$$\frac{\partial^2u}{\partial x^2}=u_{1,ii}\;;\;\frac{\partial^2u}{\partial y^2}=u_{1,jj}\;;\;\frac{\partial^2v}{\partial x^2}=u_{2,ii}\;;\frac{\partial^2v}{\partial y^2}=u_{2,jj}\;;\;\frac{\partial^2u}{\partial x\partial y}=u_{1,ij}\;;\frac{\partial^2v}{\partial x\partial y}=u_{2,ij}$$

Where, i and j, with (,) denotes the order of partial differentiation. Let δu_k $(k=1,2)$ and $\delta u_{k,ij}(k=1,2)$ be the virtual displacements, and $\delta\varepsilon_{ij}\,,\delta\kappa_{ijk}$ be the associated virtual strains. Thus, the Internal Virtual Work (IVW) of 2D composite in the framework of plane stress and assumption of small strain, $\varepsilon_{ij}=\frac{1}{2}\left(u_{i,j}+u_{j,i}\right)$ is given by (5):

$$\begin{aligned}IVW\;=\;&-\iint_{\omega\to 2D}S_{ij}\cdot\delta\left\{\frac{1}{2}\left(u_{i,j}+u_{j,i}\right)\right\}d\omega-\iint_{\omega\to 2D}\zeta_{ijk}\cdot\delta\left\{u_{1,ii}\;,\;u_{1,jj}\,,u_{1,ij}\,,\right.\\&\left.u_{2,ii}\,,u_{2,jj}\,,\;u_{2,ij}\right\}d\omega\end{aligned} \tag{5}$$

After performing integration by parts of both the terms in the above equation and using the principle of virtual work (PVW) for case of static analysis, the equilibrium equations (in weak form) of the

homogenized nonlocal theory for analysis of compressive strength of the composite in 2D can be written as follows (6):

$$\Pi = IVW + EVW = 0 \qquad \forall \delta \boldsymbol{u} \tag{6}$$

Where, External Virtual Work (EVW) is as follows (7):

$$\begin{aligned} EVW \;=\; -\Bigg\{ & \iint_{\omega} F_k \cdot \delta u_k \, d\omega \\ & + \oint_{S} f_k \cdot \delta u_k \, dS + \sum \iint_{\omega} M_k \cdot \delta u_{k,i} \, d\omega + \sum \oint_{S} m_k \cdot \delta u_{k,i} \, dS + \oint_{S} C_\tau \\ & \cdot \frac{\partial \delta u_k}{\partial n} \, dS + \sum P \, \delta u_k \Bigg\} \end{aligned} \tag{7}$$

$With\, k = 1{,}2$ and $\gamma = i \;\; or \;\; j$

Where, F_k is Body/Volume force; f_k is Traction/surface force; M_k is Couple force on the plane/body; m_k is Couple force on the edge/surface of the plane/body; C_τ is Couple spread on the edge of the plane/body, only normal at the edge of plate and P is contributions of concentrated load at the corner/edge. Consequently, the local equilibrium equations in strong form and the boundary conditions can be written as follows (8):

Equilibrium equations (Strong Form):

a) *Domain(ω)*:

$$S_{ij,j} = -F_k \quad \text{and} \quad \zeta_{ijk,ji} = -\sum M_k \qquad \forall point \;\; on \;\; \in \omega$$

b) Boundary(S):

$$\begin{aligned} -S_{ij} \cdot n_j &= -f_k && \forall point \;\; on \;\; \in S \\ \zeta_{ijk} \cdot n_\gamma \cdot n_\gamma &= -C_\tau && \forall point \;\; on \;\; \in S \\ \zeta_{ijk,j} \cdot n_\gamma + \tfrac{\sum_{i=1}^{8} \partial \zeta_{ti}}{\partial S} &= -\sum m_k && \forall point \;\; on \;\; \in S \end{aligned} \tag{8}$$

Boundary conditions(BC) on S:

Specify:

$$i) \quad u_k \quad or \quad S_{ij} \cdot n_j \quad ; \quad ii) \quad u_{k,i} \quad or \quad \zeta_{ijk} \cdot n_\gamma \cdot n_\gamma$$

Where, $k = 1{,}2 \;\; and \;\; \gamma = i, j.$

2.2 Finite element part

2.2.1 FE formulation of Non-local model (2D)

Consider Eq. 2,

$$-\int_{\Omega \to 2D} \{\boldsymbol{\zeta} \cdot \delta \boldsymbol{\kappa} + \boldsymbol{S} : \delta \boldsymbol{E}\} d\Omega + \langle \boldsymbol{F} \cdot (\delta \boldsymbol{u} \, , \delta \boldsymbol{\kappa}) \rangle = 0 \qquad \forall \delta \boldsymbol{u} \, , \forall \delta \boldsymbol{\kappa} \tag{9}$$

By expanding and neglecting the normal and corner terms, the above equation is written as (10):

$$-\int_{\Omega\to 2D}\{\overline{\overline{C_f}}\,\boldsymbol{\kappa}\,\delta\boldsymbol{\kappa}\;+\;\overline{\overline{\boldsymbol{D}}}\,\boldsymbol{\varepsilon}\;:\;\delta\boldsymbol{\varepsilon}\}d\Omega = \int_{\Omega\to 2D}\boldsymbol{f}_b\;\delta\boldsymbol{u}^T d\Omega+\int_S \boldsymbol{f}_S\;\delta\boldsymbol{u}^T\,dS+\int_{\Omega\to 2D}\boldsymbol{M}_b\;(\delta\boldsymbol{u}')^T d\Omega + \int_S \boldsymbol{M}_S\;(\delta\boldsymbol{u}')^T\,dS \quad \forall\delta\boldsymbol{u} \tag{10}$$

Where, $\overline{\overline{\boldsymbol{D}}}$ is the 4th order constitutive matrix, local fiber bending stiffness matrix, $\overline{\overline{\boldsymbol{C_f}}}$ is a diagonal matrix of size (6x6), $\boldsymbol{M}_b$ and $\boldsymbol{M}_S$ are the '*couple forces*' acting on the body and at the surface/edge and derivatives of displacement or deflection, $\boldsymbol{u}' = \left[\frac{\partial u}{\partial x},\frac{\partial u}{\partial y},\frac{\partial^2 u}{\partial x\partial y},\frac{\partial v}{\partial x},\frac{\partial v}{\partial y},\frac{\partial^2 v}{\partial x\partial y}\right]^{\boldsymbol{T}}$.

Let $\boldsymbol{d}^{(e)}$ be the DOF vector of the element and $\boldsymbol{N}$, the shape function vector for displacement then:

$$\boldsymbol{u}\cong\boldsymbol{N}\,\boldsymbol{d}^{(e)};\quad \boldsymbol{u}'\cong\boldsymbol{N}'\,\boldsymbol{d}^{(e)};$$
$$\boldsymbol{\varepsilon}\cong\boldsymbol{B}\,\boldsymbol{d}^{(e)};\quad \boldsymbol{B}=B_{ij}=[\boldsymbol{D}]\,\boldsymbol{N};\quad \boldsymbol{\kappa}\cong\boldsymbol{B}'\,\boldsymbol{d}^{(e)} \tag{11}$$

Where, $[\boldsymbol{D}]$ is a derivative operator. Now substituting above approximations in (9) and performing some mathematical steps, we get system of equations as follows:

$$-\int_{\Omega\to 2D}\{\overline{\overline{\boldsymbol{C_f}}}\,\boldsymbol{B}'\,(\boldsymbol{B}')^T\;+\overline{\overline{\boldsymbol{D}}}\,\boldsymbol{B}\;\boldsymbol{B}^T\}\;\boldsymbol{d}^{(e)}\;d\Omega = \int_{\Omega\to 2D}\boldsymbol{f}_b\;\delta\boldsymbol{N}^T\;d\Omega+\int_S\boldsymbol{f}_S\;\delta\boldsymbol{N}^T\;dS+\int_{\Omega\to 2D}\boldsymbol{M}_b\;(\delta\boldsymbol{N}')^T\,d\Omega + \int_S\boldsymbol{M}_S\;(\delta\boldsymbol{N}')^T\,dS$$

Or, Let $\boldsymbol{B}_1=\boldsymbol{B}$ and $\boldsymbol{B}_2=\boldsymbol{B}'$

$$\text{Let,}\quad \boldsymbol{K_b}=\int_{\Omega\to 2D}\{\overline{\overline{\boldsymbol{C_f}}}\,(\boldsymbol{B}_2)^T\,\boldsymbol{B}_2\;\}\,d\Omega$$
$$\boldsymbol{K_N}=\int_{\Omega\to 2D}\left\{\{\overline{\overline{\boldsymbol{D}}}\,\boldsymbol{B}_1{}^T\,\boldsymbol{B}_1\;\}\,t\;\right\}\,d\Omega \tag{12}$$

$$(\boldsymbol{K_b}+\boldsymbol{K_N})^{(e)}\;\boldsymbol{d}^{(e)}=\boldsymbol{f}^{(e)}$$

Or,

$$\Longrightarrow \boldsymbol{K}^{(e)}\;\boldsymbol{d}^{(e)}=\boldsymbol{f}^{(e)}$$

$$K_{ij}^{(e)}\;d_i{}^{(e)}=\;f_i^{(e)}$$

Where, $\boldsymbol{K}_b$ is the fiber bending stiffness and $\boldsymbol{K}_N$ is the normal/ in-plane stiffness and t is the thickness of the 2D composite plate. $\boldsymbol{B}_1$ and $\boldsymbol{B}_2$ are the normal and higher order (bending) strain displacement matrix. The above system of equations is implemented in UEL subroutine (written in FORTRAN 77), thereby developing a new C^1 continuous non-local element (NL U32) to simulate compressive strength of 2D UD ply and complex composites (carbon/epoxy long fiber) using ABAQUS ©. The numerical integration is performed by using (4x4) Gauss quadrature rule.

2.2.2 Formulation of Non-local element (NL U32)

The Lagrange elements (available in ABAQUS ©) are C^0 type continuous elements. The solution field variable (for ex: displacement,U), which is being approximated in Lagrange type of elements are only continuous between element, but not their derivatives. In order to solve the formulation of microbuckling problem using FEM accurately, it is must to have a C^1 type continuous element (Hermit type), where the solution of field variables and its derivatives are necessary. Or, in other words using Hermit type elements, the continuity between the elements is not only with the solution of field variable, but also with their derivatives (gradients), so that the microbuckling phenomenon (non-local phenomenon) can be captured well at mesoscopic level.

It is important to note that, the strain gradient quantities are the second order spatial derivatives of displacement. If we use a reference element, it is necessary to link the first and second order derivatives between two coordinate systems (global and local). Consequently, interpolation of geometry should permit to establish this link (Jacobi for first and second derivate).

Therefore, a new element (NL U32) is formulated, similar to Bogner-Fox-Schmit rectangle [21] as shown in Fig.4, where the degrees of freedom (D.O.F) of the element is not only the displacements, but also their derivatives. BFSR type element is normally used for buckling analysis of plates. See for instance [22-23].

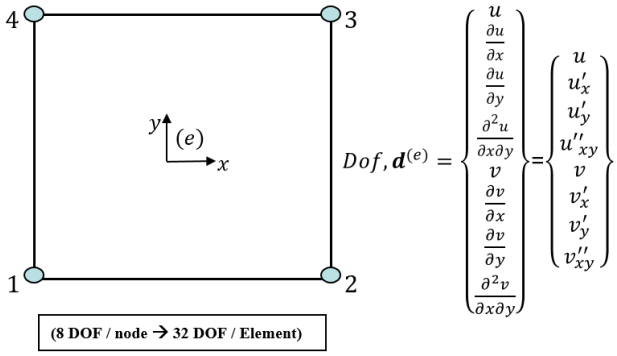

Figure 4: Non-Local Super-parametric Element (NL U32)

- **Interpolation functions:**
  (a) Displacement: Complete 3rd order cubic polynomial is chosen.

$$\begin{aligned} \boldsymbol{U}(\boldsymbol{x},\boldsymbol{y})) \cong \boldsymbol{u_h}(\boldsymbol{x},\boldsymbol{y}) = \boldsymbol{v_h}(\boldsymbol{x},\boldsymbol{y}) = {} & c_1 + c_2 x + c_3 y + c_4 x^2 + c_5 xy + + c_6 y^2 + c_7 x^3 + c_8 x^2 y \\ & + c_9 xy^2 + c_{10} y^3 + c_{11} x^3 y + c_{12} x^2 y^2 + c_{13} xy^3 + c_{14} x^3 y^2 + c_{15} x^2 y^3 \\ & + c_{16} x^3 y^3 \end{aligned} \tag{13}$$

$$\boldsymbol{u}_h(\xi,\eta) \cong \sum_{i=1}^{16} N_i^{(e)}(\xi,\eta)\,\bar{\boldsymbol{u}}_i$$

$$\boldsymbol{v}_h(\xi,\eta) \cong \sum_{i=1}^{16} N_i^{(e)}(\xi,\eta)\,\bar{\boldsymbol{v}}_i$$

Where, $\bar{\boldsymbol{u}}_i = \begin{Bmatrix} u_1 \\ u_{1,x} \\ u_{1,y} \\ u_{1,xy} \\ , \\ , \\ , \\ . \\ . \\ . \\ u_{16,xy} \end{Bmatrix}$; $\bar{\boldsymbol{v}}_i = \begin{Bmatrix} v_1 \\ v_{1,x} \\ v_{1,y} \\ v_{1,xy} \\ , \\ , \\ , \\ . \\ . \\ . \\ v_{16,xy} \end{Bmatrix}$

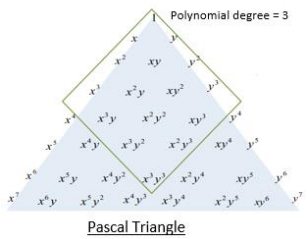

- 1D cubic Hermit type polynomials are used:

$$H_{01}(\xi) = 1 - 3\left(\frac{\xi+1}{2}\right)^2 + 2\left(\frac{\xi+1}{2}\right)^3 \qquad H_{01}(\eta) = 1 - 3\left(\frac{\eta+1}{2}\right)^2 + 2\left(\frac{\eta+1}{2}\right)^3$$
$$H_{02}(\xi) = 3\left(\frac{\xi+1}{2}\right)^2 - 2\left(\frac{\xi+1}{2}\right)^3 \qquad H_{02}(\eta) = 3\left(\frac{\eta+1}{2}\right)^2 - 2\left(\frac{\eta+1}{2}\right)^3$$
$$H_{11}(\xi) = \left(\frac{\xi+1}{2}\right) - 2\left(\frac{\xi+1}{2}\right)^2 + \left(\frac{\xi+1}{2}\right)^3 \qquad H_{11}(\eta) = \left(\frac{\eta+1}{2}\right) - 2\left(\frac{\eta+1}{2}\right)^2 + \left(\frac{\eta+1}{2}\right)^3$$
$$H_{12}(\xi) = \left(\frac{\xi+1}{2}\right)^3 - \left(\frac{\xi+1}{2}\right)^2 \qquad H_{12}(\eta) = \left(\frac{\eta+1}{2}\right)^3 - \left(\frac{\eta+1}{2}\right)^2$$

The above 1D polynomials permits to build displacement interpolation functions as follows(14):

$$N_j = \left[\ H_{0i}(\xi)\ H_{0i}(\eta)\ ;\ H_{1i}(\xi)\ H_{0i}(\eta)\ ;\ H_{0i}(\xi)\ H_{1i}(\eta)\ ;\ H_{1i}(\xi)\ H_{1i}(\eta)\ \right] \qquad (14)$$
$$where, j = 1, \ldots.16\ and\ i = 0,1,2$$

The obtained shape functions corresponds to 32 D.O.F of the element. For detailed formulation of shape functions refer for instance [21].

(b) Geometry: Complete 2nd order biquadratic polynomial is chosen in order to calculate the second derivatives in Jacobi as discussed earlier.

$$x \cong \sum_{j=1}^{9} N_j^{(e)}(\xi,\eta)x_i$$
$$y \cong \sum_{j=1}^{9} N_j^{(e)}(\xi,\eta)y_i$$

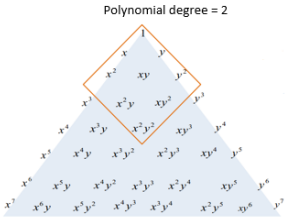

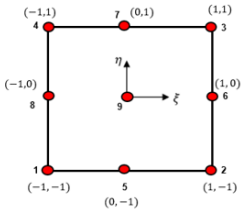

Abaqus UEL workflow:

UEL (User Elements) subroutine is a programming interface provided with ABAQUS ©/Standard using which one can define customized finite elements. It is very important to understand the overall operation of the 'UEL' block. Fig. 5 shows a schematic describing the 'input' and 'output' flow from the UEL subroutine, that is called for every element. For a current time increment, ABAQUS © provides the incremental and final nodal point displacements. State variables (stress/strain) at the start of that time increment are also provided. UEL is then required to return the updated element stiffness matrix (AMATRX), internal force (RHS) and state variables all at the end of the current time step [25].

Figure 5: I/O block diagram for UEL subroutine

The UEL is built under an incremental form, this makes us easier to integrate non-linear behavior laws in future. User Material subroutines: 'UMAT' and 'URMAT' should be introduced in order to calculate the tangent behavior of 2D classical stiffness (UMAT) and non-local stiffness (URMAT).

3 Results

3.1 Validation of NL U32 element

In order to compare the accuracy and validate Non-Local element (NL U32) for linear elastic isotropic case, results are compared with ABAQUS © linear plane stress element (CPS4), as it is much more convenient reference element at the moment, since it is also built with plane stress formulation. The values of $\overline{\overline{C_f}}$ parameters (A, B, C, D, E, F) is unknown for NL U32 element. Therefore, it is important to understand the influence of these parameters on the solution. Hence, $\overline{\overline{C_f}}$ parameters value are varied and kept constant in all the cases. Results of only few relevant test cases are presented here.

It should be noted that for all the cases, same material properties has been defined for CPS4 element: Elastic Young's modulus, $E = 2.0E5\ MPa$, Poisson's ratio, $\nu = 0.3$ and thickness, $t = 1mm$. For NL U32 element, material properties are: Matrix Young's modulus, $E_m = 2.0E5\ MPa$, Poisson's ratio, $\nu_m = 0.3$, thickness, $t = 1mm$, the values for parameters of local fiber bending stiffness matrix A, B, C, D, E, F: started with initial guess of low value, $0.15\ MPa \cdot mm^2$ and varied with the order of 100. Analysis is performed on a rectangular plate (100 x 50 mm), meshed with 276 Elements (312 nodes).

Case1: Compression

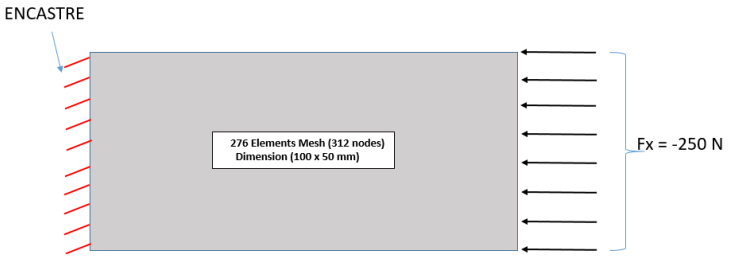

Figure 6: Mesh, Load and Boundary conditions

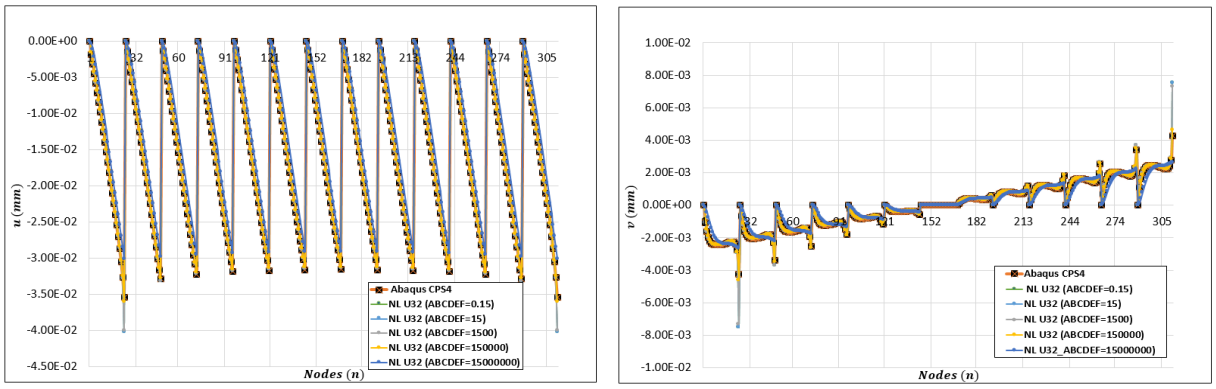

Figure 7: Influence of Cf Parameters

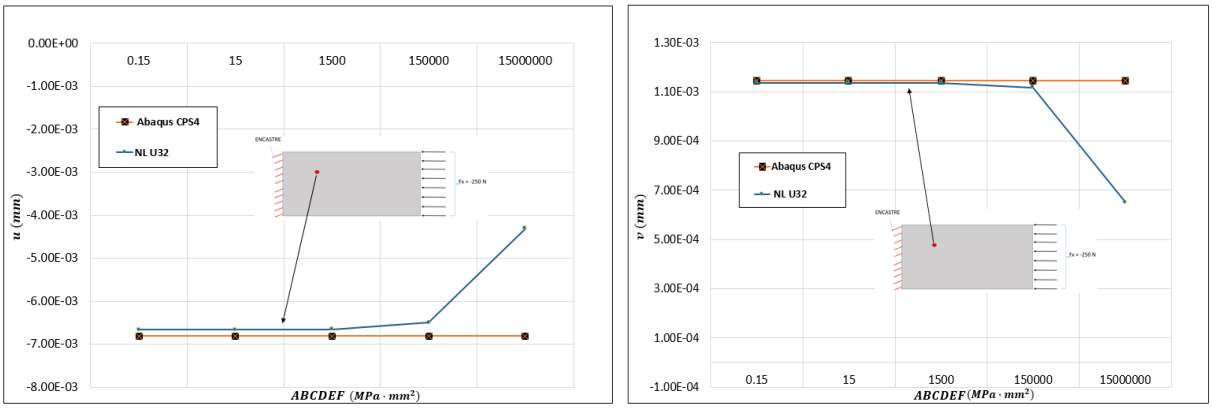

Figure 8: Comparison of Displacements (u,v) at node 222 for different Cf parameters value

Case2: Bending

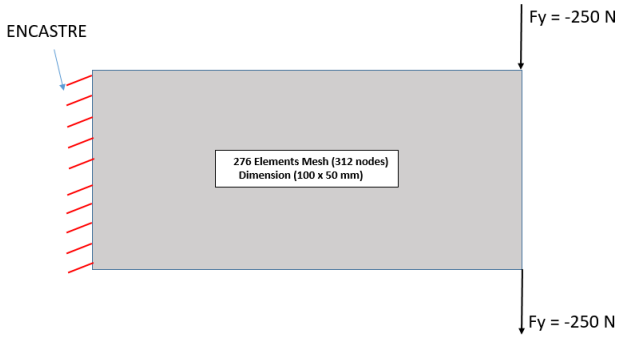

Figure 9: Mesh, Load, and Boundary Conditions

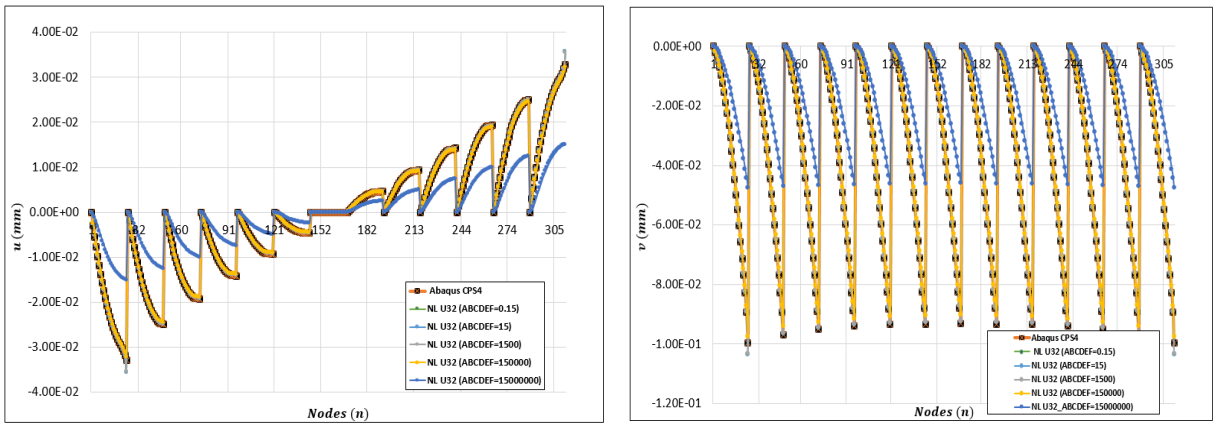

Figure 10: Influence of Cf Parameters

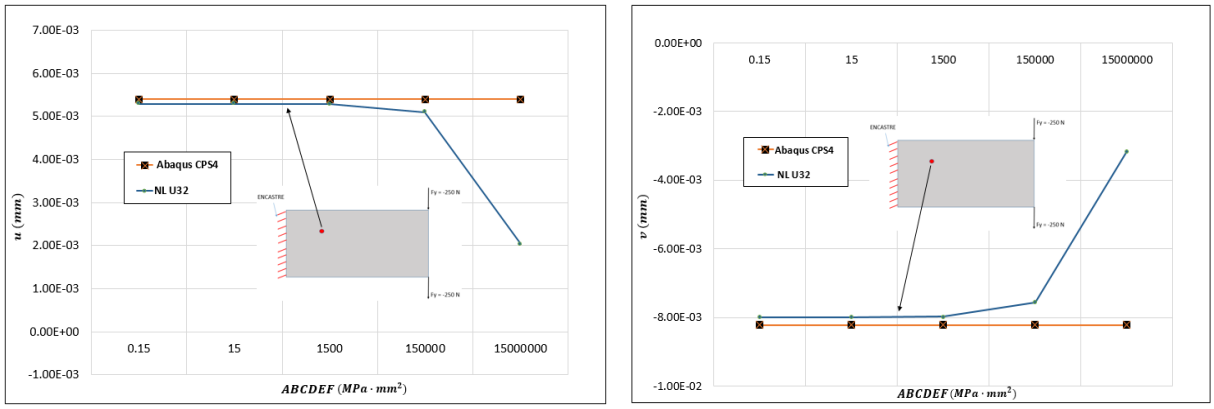

Figure 11: Comparison of Displacements (u,v) at node 222 for different Cf parameters value

From both the cases: compression (Fig. 7) and bending (Fig. 10), it can be observed that, similar response and difference in solution is very less compared to ABAQUS © CPS4 element when local fiber bending stiffness matrix, $\overline{\overline{\boldsymbol{C_f}}}$ parameters (ABCDEF) varied up to 1500 $MPa \cdot mm^2$. But, significant difference in solution is observed compared to CPS4 element when ABCDEF value is increased above 1500 $MPa \cdot mm^2$ (see Fig. 8 and Fig. 11). Much stiffer response can be observed with NL U32 compared to continuum solid CPS4. This is because, for lower order of $\overline{\overline{\boldsymbol{C_f}}}$ ($\leq 10^3$), the order of bending energy ($\boldsymbol{\kappa}^T \overline{\overline{\boldsymbol{C_f}}}\, \boldsymbol{\kappa}$) becomes lower compared to classical strain energy ($\boldsymbol{\varepsilon}^T\, \bar{\bar{\boldsymbol{D}}}\, \boldsymbol{\varepsilon}$), since the order of curvatures is also lower. Consequently, bending energy has negligible contribution to the total energy. So, we tend to obtain similar solution as classical plane stress solution. But, for higher order of $\overline{\overline{\boldsymbol{C_f}}}$ ($> 10^3$), the order of bending energy becomes similar or higher compared to the classical strain energy. Consequently, we can observe significant difference in solution for ABCDEF >1500 $MPa \cdot mm^2$. The level of stiffness which generates an effect, can be estimated (but not shown here), and we have also obtained the value of 1500 $MPa \cdot mm^2$. In conclusion, in order to have non-local effects in this particular solution, it is necessary to have $\overline{\overline{\boldsymbol{C_f}}}$ parameters value $> 10^3$. This clearly explains the influence of $\overline{\overline{\boldsymbol{C_f}}}$ parameters value in the solution. In future, it is necessary to obtain proper values for ABCDEF in correspondence to a composite mesostructure. It is also important to note that, the choice of interpolation functions, integration rule for both ABAQUS © CPS4 and NL U32 element are different, which can also cause difference in solution, especially near the points of loading. However, the global response obtained with NL U32 is almost similar compared to ABAQUS © CPS4 element, which validates the non-local element for linear isotropic elastic case.

<u>Mesh Convergence study:</u>

In order to understand the convergence of the solution obtained with NL U32 element against mesh size, various mesh size of: $no.of\ elements, n = 8, 32, 66, 128, 276, 512$ is chosen. The material properties, loading and boundary conditions is same as previous (case 2), except that the two values of ABCDEF is chosen: 15 $MPa \cdot mm^2$ and 1500000 $MPa \cdot mm^2$. The solution is compared with ABAQUS © CPS4 element. We can observe from Fig. 12, that as the mesh size (n) is increased, we tend to obtain an asymptotic or converged solution for both NL U32 element and ABAQUS © CPS4 element. As discussed earlier, for lower values of ABCDEF with increase in mesh size, we tend to obtain similar solution as classical plane stress element CPS4, and for higher values of ABCDEF, quite significant difference can be observed. However, the convergence is obtained with increase in mesh size. This confirms that for finer mesh, we will obtain a good converged solution with NL U32 element.

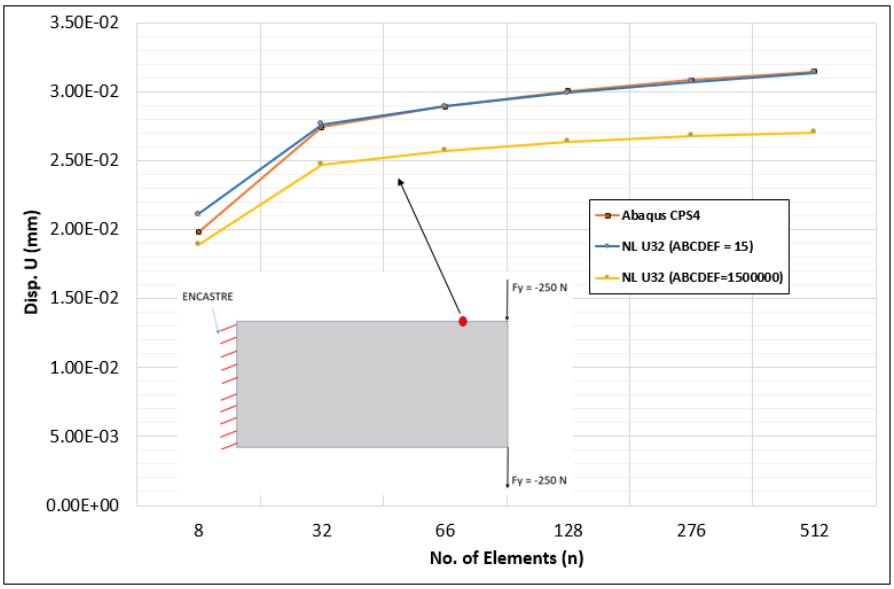

Figure 12: Mesh Convergence study of NL U32 element

3.2 Comparison with 2D heterogeneous complete microstructure

3.2.1 Methodology

As a final step of validation of Non-Local Homogeneous model implemented in non-local element (NL U32) for linear elastic case, results are compared with 2D Unidirectional (UD) composite (T300/914 Carbon/epoxy) model built using Abaqus plane stress element (CPS4). The stacking sequence of UD heterogeneous composite (with 10 layers) model built in Abaqus is as shown in (Fig. 13):

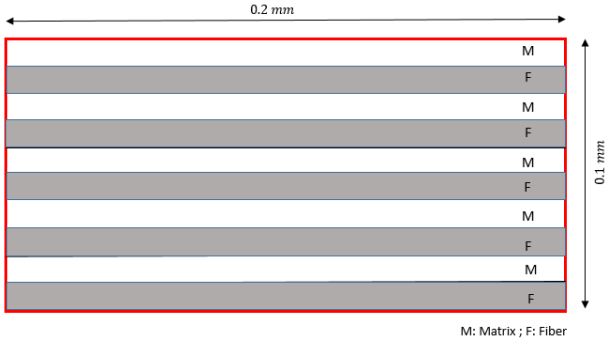

Figure 13: 2D composite stacking sequence: UD plies at 0^0

The elastic properties of T300/914 Carbon/epoxy UD ply obtained from [18] as in Table. 1 is assigned for both matrix and fiber in heterogeneous model of Abaqus and homogenous non-local model. Note that the matrix and fiber is assumed isotropic in both the models.

Table 1: Material properties of UD ply [18]

Heterogeneous model Abaqus (CPS4)		**Homogenous Non-local model (NL U32)**	
matrix	fiber	matrix	fiber
$E_m = 4500\ Mpa$	$E_f = 24000\ Mpa$	$E_m = 4500\ Mpa$	$E_f = 24000\ Mpa$
$\nu_m = 0.4$	$\nu_f = 0.3$	$\nu_m = 0.4$	$\nu_f = 0.3$
thickness, $t = 1mm$		Volume fraction, $f = 0.625$	
		Diameter of fibers, $d_f = 0.01mm$	
		Local fiber bending stiffness parameter for UD ply, $D = fE_f r_{gf}^2 = 0.09375\ MPa \cdot mm^2$	*fiber gyration radius,* $r_{gf} = \sqrt{\frac{I}{S_f}}$
		ABCEF = 0.001*D	thickness, $t = 1mm$

It is important to note that, for UD ply, since there is just one gradient ($v'' = \frac{\partial^2 v}{\partial x^2}$) along thickness direction, as in case of [2], just one parameter (D) of local bending stiffness matrix, $\overline{\overline{C_f}}$ is considered, values for other parameters (ABCEF) is assigned very low compared to parameter D in homogenous non-local model.

3.2.2 Results

From Fig. 14 and Fig. 15, it is clear that the results (displacements: u, v) obtained from homogenous non-local model is in close comparison with the results of heterogeneous model of ABAQUS © for the case of UD composite subjected to bending. The slight difference between two solutions are clearly due to the addition of non-local terms and choice of interpolation functions (for displacement and geometry) in homogenous non-local model. With this validation, it can be concluded that the homogenized non-local model (implemented in NL U32 element) can be used for analysis of UD composites (linear isotropic elastic cases).

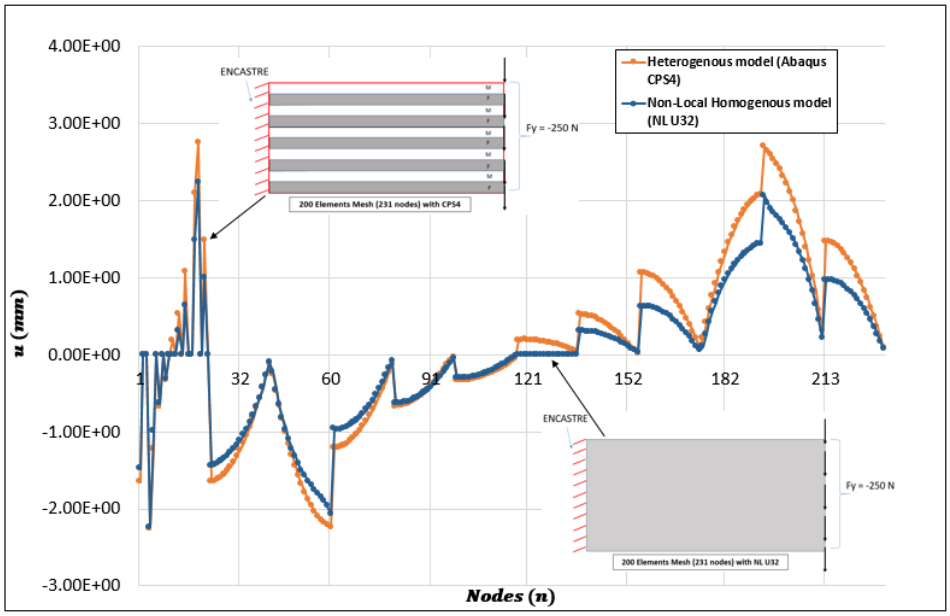

Figure 14: comparison of variation of displacement (u) over nodes

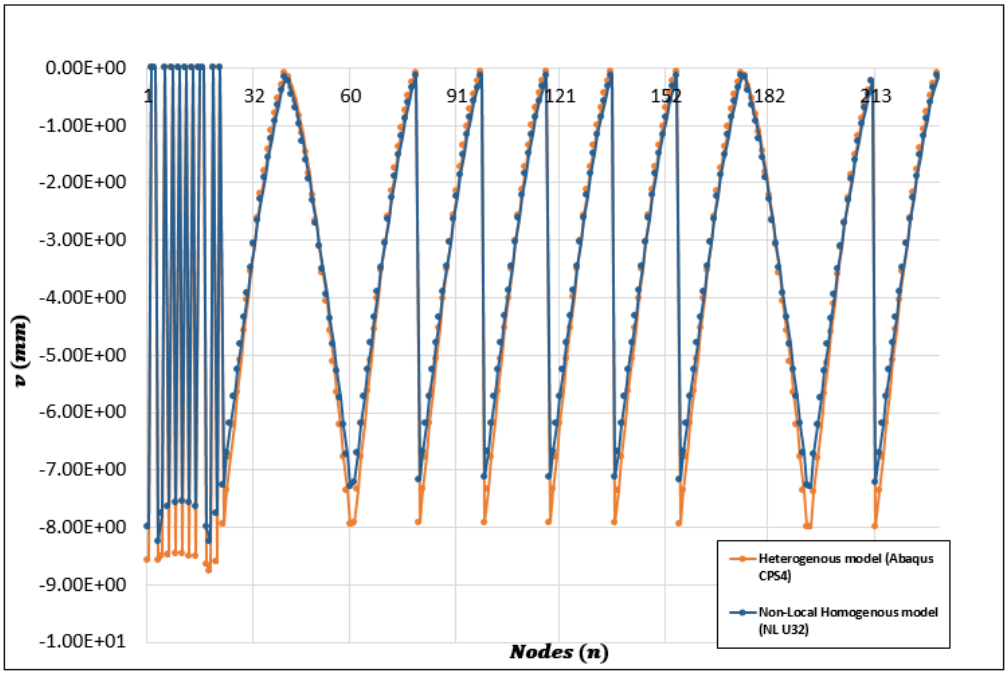

Figure 15: comparison of variation of displacement (v) over nodes

4 Conclusion

A homogenized non-local finite element model has been proposed, similar to Mindlin' second gradient theory [1] and the first numerical developments have been initiated. The framework of this nonlocal modeling is more general that of [2] to assess microbuckling phenomenon in UD and complex composites (carbon/epoxy long fiber) at the structural/mesoscopic scale. The developed non-local numerical model is implemented in User Element (UEL) subroutine for analysis in ABAQUS ©, thereby developing a 2D, C^1 continuous non-local super-parametric element (NL U32) for linear isotropic elastic case. Various tests results are presented to validate the capability of NL U32 element in comparison with ABAQUS © iso-parametric plane stress element (CPS4) and also to understand the influence of $\overline{\overline{\boldsymbol{C_f}}}$ parameters. In addition, as a final check for validation, the non-local homogenous 2D model implemented in NL U32 is compared with complete 2D UD heterogeneous composite structure, modeled using ABAQUS © CPS4 element. From all the test cases, good results are obtained in comparison with the ABAQUS © iso-parametric element, thereby validating the capability of non-local element (NL U32).

However, since no non-linear effects (material and geometrical) are included in NL U32 element, it is not possible to assess the actual microbuckling phenomenon in UD and woven composites at the moment, the values of $\overline{\overline{\boldsymbol{C_f}}}$ parameters are also unknown. Hence, in future it is planned to implement non-linear effects in the model, consequently in NL U32 element for 2D case. Along with obtaining the optimized $\overline{\overline{\boldsymbol{C_f}}}$ parameters values by comparing simulations between complete microstructure and non-local simulations and finally extension to develop 3D non-local element to assess 3D woven composites.

Références

[1] R.D. Mindlin, Microstructure in linear elasticity, Arch. Rat. Mech. Anal 16 (1964) 57-78.
[2] S. Drapier, J.-C. Grandidier, M. Potier-Ferry, Towards a numerical model of the compressive strength for long fiber composites, European Journal of Mechanics /A Solids 18 (1999) 69-92.
[3] P.-Y. Méchin, V. Keryvin, J.-C. Grandidier, D. Glehen, An experimental protocol to measure the parameters affecting the compressive strength of CFRP with a fibre micro-buckling failure criterion, Composite Structures 211 (2019) 154-162.
[4] J.W. Hutchinson, T.Y. Wu (Eds), Advances in applied mechanics. Academic Press (1997) 33, 296-361.
[5] M. R. Wisnom, The effect of the specimen size on the bending strength of unidirectional carbon fiber-epoxy. Comp. Struct (1991). 18, 47-63.
[6] C. Gardin, M. Poitier-Ferry, Microflambage des fibers dans un matériaux composite à fibers longues: analyse asymptotique 2-D. Compt. Rend. de l'Acad. des Sci. Paris (1992) Série II 315, 1159-1164.
[7] I. Grandsire-Vincon, Compression des Composites Unidirectionnels: Méthodes d'Essais et Approche Micréchanique. Thése de Doctorat de l'ENS Cachan.
[8] B.N. Cox, M.S. Dadkhah, W.L. Morris, J.G. Flintoff, Failure mechanisms of 3D woven composites in tension, compression and bending. Acta. metall. Mater (1994) 42(12), 3967-3984.
[9] M. Abdel Ghafaar, A.A. Mazen, N.A. El-Mahallawy, Behavior of woven fabirc reinforced epoxy composites under bending and compressive loads. Journal of Engg. Sci. (2006) 34(2), 453-469.
[10] K.C. Warren, R.A. Lopez-Anido, J. Goering, Experimental investigation of three- dimensional woven composites. Composites Part A Applied sci. and Manufact. (2015a) 73, 242-259.
[11] B.W. Rosen, Mechanics of Composite Strengthening, Fibre Composite Materials, American Society of Metals Seminar, Metals Parks, Ohio (1964) 37-75.
[12] A.S. Argon, Fracture of Composites. Treatise of Materials Science and Technology, vol.1, Academic Press, New York (1972).
[13] B. Budiansky, N.A. Fleck, Compressive failure of fibre composite, J. Mech. Phys. Solids (1993) 41 (1), 183-211.
[14] N.A. Fleck, L. Deng, B. Budiansky, Prediction of kink width in fiber composite. J. 41 Appl. Mech. (1995a) 62, 329-337.
[15] W.J. Schaffrers, Buckling in fiber reinforced elastomer. Text. Res. J. (1977) 502-512.
[16] S.R. Swanson, A micromechanics model for in-situ compression strength of fiber composite laminates. ASME J. Engng. Mat. Technol. (1992) 114, 8-12.
[17] J.-C. Grandidier, G. Ferron, M. Potier-Ferry, Microbuckling and strength in long-fiber composites: theory and experiments. Int. J. Solids Struct. (1992) 29(14/15), 1753-1761.
[18] S. Drapier, J.-C. Grandidier, C. Gardin, M. Potier-Ferry, Structure effect and microbuckling, Composite Science and Technology (1996) 56, 861-867.
[19] S. Nezamabadi, M. Poitier-Ferry, H. Zahrouni, J. Yvonnet, Compressive failure of composites: A computational homogenization approach, Composites structures (2015) 127, 60-68.
[20] S. Drapier, J.-C. Grandidier, M. Potier-Ferry, A structural approach of plastic microbuckling in long fiber composites: comparison with theoretical and experimental results, Composite Science and Technology (2001) 38, 3877-3904.
[21] F.K. Bogner, R.L. Fox and L. A. Schmit, The Generation of Inter-element Compatible Stiffness and Mass Matrices by the Use of Interpolation Formulas, Proceedings of the Conference on Matrix Methods in Structural Mechanics, Wright-Patterson Air Force Base, Ohio, October (1965) 397-444.
[22] A. Pifko, G. Isakson, A Finite element method for plastic buckling analysis of plates. AIAA Journal (1969) 7(10), 1950-1957.

[23] N.K. Naik, R. Ramasimha, Estimation of compressive strength of delaminated composites. Composites structures (2001) 52(2), 199-204.
[24] K. Berkache, S. Deogekar, I. Goda, R.C. Picu, J.-F. Ganghoffer. Construction of second gradient continuum models for random fibrous networks and analysis of size effects. Composites structures (2017) 181, 347-357.
[25] Abaqus 6.10 user's manual (Section 1.1.23 and 29.16.1). Retrieved from https://www.sharcnet.ca/Software/Abaqus610/Documentation/docs/v6.10/books/sub/default.htm?startat=ch01s01asb23.html#sub-rtn-uuel